Chinese Chemical Letters 31 (2020) 2641–2644

Contents lists available at ScienceDirect

Chinese Chemical Letters

journal homepage: www.elsevier.com/locate/cclet

Communication

# Cable-like carbon nanotubes decorated metal-organic framework derived ultrathin $CoSe_2$/CNTs nanosheets for electrocatalytic overall water splitting

Guijuan Wei[a,1], Kun Du[b,1], Xixia Zhao[a], Jiayang Wang[b], Wenxiu Yan[b], Chao An[b], Changhua An[b,*]

[a] State Key Laboratory of Biobased Material and Green Papermaking, Qilu University of Technology, Shandong Academy of Sciences, Jinan 250353, China
[b] Tianjin Key Laboratory of Organic Solar Cells and Photochemical Conversion, School of Chemistry and Chemical Engineering, Tianjin University of Technology, Tianjin 300384, China

ARTICLE INFO

*Article history:*
Received 14 January 2020
Received in revised form 4 February 2020
Accepted 14 February 2020
Available online 15 February 2020

*Keywords:*
$CoSe_2$
Carbon nanotubes
Ultrathin
Bifunctional electrocatalyst
Water splitting

ABSTRACT

The high cost and low reserves of noble metals greatly hinder their practical applications in new energy production and conversion. The exploration of cost-effective alternative electrocatalysts with the ability to drive hydrogen evolution reaction (HER) and oxygen evolution reaction (OER) is extremely significant to promote overall water splitting. Herein, ultrathin $CoSe_2$/CNTs nanocomposites have been synthesized by a facile two-step method, where the ultrathin Co-MOF (metal organic-framework) decorated with cable-like carbon nanotubes (CNTs) (Co-MOF/CNTs) was initially fabricated, and followed a low-temperature selenization process. The ultrathin $CoSe_2$ nanosheets as well as the superior conductivity of CNTs synergistically resulted in abundant active sites and enhanced conductivity to boost the electrocatalytic activity. The as-prepared $CoSe_2$/CNTs electrocatalysts exhibited an overpotential of 190 mV and 300 mV *vs.* reversible hydrogen electrode (RHE) at a current density of 10 mA/cm$^2$ for the HER and OER in alkaline solution, respectively, and demonstrated superior durability. Furthermore, the as-prepared bifunctional $CoSe_2$/CNTs electrocatalysts can act as cathode and anode in an electrolyzer, showing a cell voltage of 1.75 V at 10 mA/cm$^2$ for overall water splitting.


Electrocatalytic water splitting into hydrogen and oxygen represents one of the most promising strategies to store renewable energy and mitigate environmental issues [1–3]. Platinum-based material exhibits excellent hydrogen evolution reaction (HER) performance [4,5], meanwhile $RuO_2$ and $IrO_2$ are benchmark electrocatalysts for oxygen evolution reaction (OER) [6]. The high price and low abundance of precious metals greatly hamper their practical applications [7,8]. Furthermore, the use of different catalysts in HER and OER adds a complex process and additional equipment to manufacture electrodes. Therefore, rational design of cheap metal-based catalysts towards OER and HER is highly desirable. The integration of cathode and anode in the same electrolyte cell is beneficial for the enhanced energy efficiency and concurrently reduced manufacturing cost.

Transition metal-based electrocatalysts have attracted intensive interests due to their rich reservoir, and moderate overpotentials for water splitting whatever under both acidic or alkaline conditions [9–11]. For example, $CoSe_2$ nanoparticles exhibited excellent HER performance among first-row transition-metal (*e.g.*, Fe, Co, Ni) dichalcogenides [12]. Molecular orbital theory predicted that $CoSe_2$ acts as a promising OER electrocatalyst to promote rapid proton transfer [13]. The increase of active sites and conductivity is crucial to improve its electrocatalytic performance. Xie and co-workers showed that the OER performance of $CoSe_2$ can be improved by reducing thickness into the atomic scale to expose active edge sites [14]. Kang *et al.* incorporated carbon nanotubes (CNTs) with $CoSe_2$ microspheres, displaying an HER overpotential of ~174 mV at 10 mA/cm$^2$ in 0.5 mol/L $H_2SO_4$ [15]. Despite these advances, the facile fabrication of integrated catalyst of ultrathin $CoSe_2$ nanostructures and conductive networks for overall water splitting still remains a challenge.

Herein, ultrathin $CoSe_2$/CNTs nanocomposites have been prepared by selenization of CNTs decorated Co-MOF nanosheets. The obtained ultrathin $CoSe_2$ is favorable for exposing active sites,

* Corresponding author.
*E-mail address:* anch@tjut.edu.cn (C. An).
[1] These two authors contributed equally to this work.

https://doi.org/10.1016/j.cclet.2020.02.029
1001-8417/

and the cable-like CNTs anchored on the $CoSe_2$ nanosheets facilitate the electron-transfer. As expected, the ultrathin $CoSe_2$/CNTs nanocomposites exhibited enhanced performance towards HER and OER compared to bare $CoSe_2$ nanosheets, at low overpotential of 190 mV and 300 mV *vs.* reversible hydrogen electrode (RHE), respectively. Furthermore, a water electrolyzer equipped with two $CoSe_2$/CNTs electrodes showed good performance at a potential of 1.75 V at 10 mA/cm$^2$ for overall water splitting.

Fig. 1a illustrates the process for the preparation of ultrathin $CoSe_2$/CNTs. Firstly, Co-MOF/CNTs precursor was synthesized by reacting $Co^{2+}$ with 2-methylimidazole in CNTs dispersion of DMF at room temperature. In this process, the strong electrostatic interaction between $Co^{2+}$ ions and negative charged CNTs plays a crucial role on the heterogeneous nucleation of Co-MOF crystals on CNTs surface [16]. Subsequently, an *in-situ* selenization was introduced to convert Co-MOF/CNTs into $CoSe_2$/CNTs under Ar atmosphere at 350 °C.

The crystalline structures of as-prepared materials were analyzed by X-ray diffraction (XRD). After the selenization of Co-MOF and Co-MOF/CNTs, the Co-MOF samples can be readily transformed to the orthorhombic $CoSe_2$, which well-matched the standard pattern (JCPDS No. 53-0449) (Fig. 1b). Furthermore, Raman spectra as shown in Fig. 1c reveal the $CoSe_2$/CNTs nanocomposites have seven vibration peaks at 195, 471, 514, 605, 671, 1350, and 1591 cm$^{-1}$, respectively. The strong peaks at 195 and 671 cm$^{-1}$ are assigned to $A_g$ and $A_{1g}$ modes of $CoSe_2$ [17]. The weak peaks at 471, 514, and 605 cm$^{-1}$ could be ascribed to $E_g$, $F^1_{2g}$, and $F^2_{2g}$ modes of $CoO/Co_3O_4$, which may be caused by slight oxidation of $CoSe_2$ with trace $SeO_2$ in Se source. Besides, the peaks at 1350 cm$^{-1}$ (D-band) and 1591 cm$^{-1}$ (G-band) in the Raman spectra of $CoSe_2$/CNTs are derived from $sp^3$- and $sp^2$-hybridized carbons of CNTs [18,19], indicating the presence of CNTs. To determine the proportions of each component, the thermogravimetric (TG) curves (Fig. S1a in Supporting information) of $CoSe_2$ and $CoSe_2$/CNTs were recorded under an $O_2$ atmosphere. In the TG curve (Fig. S1a, black line) of bare $CoSe_2$, the initial weight increase at ~460 °C and a subsequent weight loss are ascribed to the partial oxidation of $CoSe_2$ and the complete oxidation into $Co_3O_4$, respectively. As for the TG curve (Fig. S1a, red line) of $CoSe_2$/CNTs nanocomposites, the first weight increase is not obvious owing to the combustion of CNTs at around 400 °C. Based on the TG results, the CNTs content in $CoSe_2$/CNTs nanocomposites was estimated to be about 19.4%, showing that the $CoSe_2$ was totally transformed into $Co_3O_4$. As shown in Fig. S1b (Supporting information), the XRD patterns of two samples obtained after the TG test are in good agreement with those of pure $Co_3O_4$ (JCPDS No. 43-1003).

Fig. 2 gives the shape microstructures of the as-prepared Co-MOF/CNTs and $CoSe_2$/CNTs. As shown in Fig. 2a and Figs. S2a-c (Supporting information), the Co-MOF exhibits nanosheets and the CNTs are tightly anchored on the Co-MOF surfaces. After selenization, the Co-MOF/CNTs has been totally converted to $CoSe_2$/CNTs with inherit of original shape (Fig. 2b and Figs. S2d-f in Supporting information). As shown in Fig. S3 (Supporting information), the size of the $CoSe_2$ in the $CoSe_2$/CNT composite is in a range of 100–300 nm, and the diameter of the CNTs is mainly focused on the 25 nm. Transmission electron microscopy (TEM) image in Fig. 2c reveals that the $CoSe_2$ in $CoSe_2$/CNTs displays ultrathin nanosheets and interconnects with CNTs. Corresponding high-resolution TEM (HRTEM) image (Fig. 2d) shows the lattice spacing of 0.26 nm, which can be assigned to the (101) crystal planes of $CoSe_2$, while the lattice spacing of 0.34 nm is for CNTs, confirming the close interaction between $CoSe_2$ and CNTs. The elemental mappings of $CoSe_2$/CNTs (Fig. 2e) show the uniform distribution of Co, Se and the presence of C element. This structure is very favorable for water splitting, where the conductivity could be enhanced by conductive CNTs networks, and the ultrathin feature of $CoSe_2$ could increase the active sites.

X-ray photoelectron spectroscopy (XPS) was carried out to investigate the chemical composition and the surface electronic state of the as-prepared $CoSe_2$/CNTs. As shown in Fig. S4a (Supporting information), the XPS survey spectrum gives the presence of Co, Se, C and O. The high resolution Co $2p_{3/2}$ peak in Fig. S4b (Supporting information) can be deconvoluted into two chemical states at the binding energies of 780.9 eV and 785.4 eV, which are from Co-Se and the shakeup satellite peak, respectively [20,21]. The Se 3d spectrum of the $CoSe_2$/CNTs (Fig. S4c in Supporting information) shows the core-level band of the Se region, in which the binding energies of Se $3d_{3/2}$ and Se $3d_{5/2}$ at 55.3 eV and 56.1 eV are coincided with $CoSe_2$, respectively [22]. The peak at around 60.2 eV is associated with $SeO_x$, which may be caused by inevitably slight oxidation of $CoSe_2$ [23], while the peaks

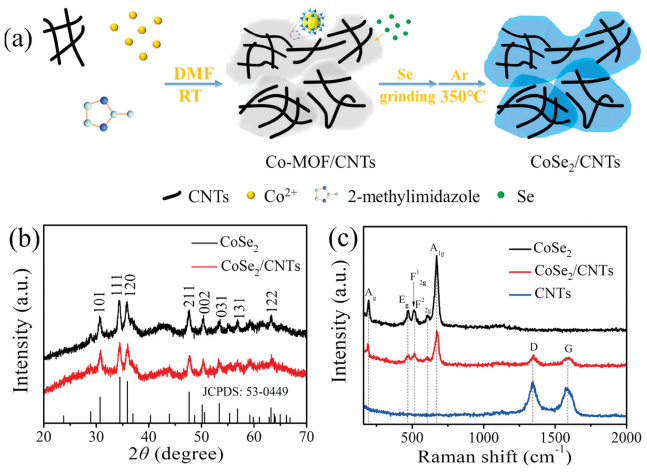


**Fig. 1.** (a) Schematic illustration for the synthesis of $CoSe_2$/CNTs nanocomposites. (b) XRD patterns of $CoSe_2$ and $CoSe_2$/CNTs with the standard pattern of $CoSe_2$ highlighted by sticks. (c) Raman spectra of $CoSe_2$, $CoSe_2$/CNTs and CNTs.

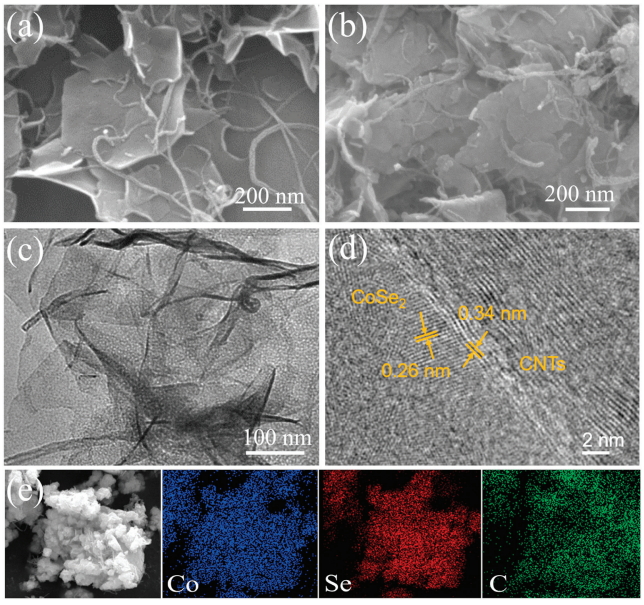


**Fig. 2.** SEM images of Co-MOF/CNTs (a) and $CoSe_2$/CNTs (b). Low-magnification (c) and high-resolution (d) TEM images of as-prepared $CoSe_2$/CNTs. (e) EDS elemental mapping of $CoSe_2$/CNTs.

in the range of 58–60 eV are attributed to Co 3p at the surface of $CoSe_2$/CNTs [24]. The C1s spectrum in Fig. S4d (Supporting information) presents the peaks of the C element, in which the peaks located at 284.8 eV, 285.6 eV, and 289.6 eV assigned to chemical bonds C—C, C–O, and C=O, respectively [25].

The electrocatalytic HER performance of the as-prepared catalysts was evaluated in 1 mol/L KOH solution with a typical three-electrode system. Fig. 3a shows their linear sweep voltammograms (LSV) lines with a scan rate of 10 mV/s. $CoSe_2$/CNTs required a lower overpotential ($\eta$ = 190 mV *vs.* RHE) to achieve the current density of 10 mA/cm$^2$ with respect to bare $CoSe_2$ ($\eta$ =266 mV *vs.* RHE), which is better than most reported $CoSe_2$-based eletrocatalysts (Table S1 in Supporting information). No HER activity was observed over CNTs. Additionally, the electrocatalytic activities of $CoSe_2$/CNTs with different CNTs contents were systematically investigated. As shown in Fig. S5a (Supporting information), the introduction of CNTs could boost the electrochemical performance effectively. With the increase of CNTs to 5 mg, the $CoSe_2$/CNTs exhibits overpotential of 190 mV, which is much lower than those of $CoSe_2$/CNTs-3 mg (194 mV) and $CoSe_2$/CNTs-8 mg (208 mV), respectively. Fig. 3b compares the Tafel slopes of $CoSe_2$/CNTs and bare $CoSe_2$. The Tafel slope over $CoSe_2$/CNTs (40 mV/dec) is much smaller than that of bare $CoSe_2$ (62 mV/dec), indicating that the HER rate on $CoSe_2$/CNTs would be more rapidly than bare $CoSe_2$. Electrochemical impedance spectroscopy (EIS) spectra (Fig. 3f) also confirm that $CoSe_2$/CNTs possessed a lower $R_{ct}$ value than bare $CoSe_2$. Thus the small Tafel slope and $R_{ct}$ value verify the accelerated reaction kinetics and enhanced conductivity over $CoSe_2$/CNTs. The synergistic effect between $CoSe_2$ and CNTs should result in the enhanced electrocatalytic activity, in which $CoSe_2$ is responsible for the HER activity, and CNTs anchored on $CoSe_2$ nanosheets offers conductive channels. Moreover, as shown in Figs. 3c and d, both LSV polarization curve after 1000 cycles and continuous amperometric *i-t* test for 20 h indicate its superior stability.

In order to further understand the enhanced catalytic activity, the electrochemical active surface areas of $CoSe_2$/CNTs and $CoSe_2$ were estimated from the cyclic voltammetry (CV) at various scan rates in a potential rage of 0.1–0.2 V. As shown in Fig. S6 (Supporting information), all the CV curves of two samples are almost rectangular, indicating their ideal capacitive behaviors in electrochemical reactions [26–28]. As revealed in Fig. 3e, a linear trend was acquired in the corresponding current density against scan rate plots for both $CoSe_2$ and $CoSe_2$/CNTs, and the capacitance values ($C_{dl}$) can be derived from the slope of the linear region. Obviously, $CoSe_2$/CNTs has a larger $C_{dl}$ of 4.5 mF/cm$^2$ compared to $CoSe_2$ (1.6 mF/cm$^2$), indicating $CoSe_2$/CNTs possesses larger electrochemical surface area with more active sites than bare $CoSe_2$. In addition, the electrochemically active surface area (ESCA) values of the $CoSe_2$/CNTs and $CoSe_2$ are determined to be 7.95 cm$^{-2}$ and 2.83 cm$^{-2}$, respectively. Intrinsic HER activity of the $CoSe_2$/CNTs and $CoSe_2$ was normalized by ESCA at 10 mV/s (Fig. S7 in Supporting information), the introduction of cable-like CNTs greatly improve the intrinsic HER activity.

The OER performance of $CoSe_2$/CNTs was evaluated in 1 mol/L KOH saturated with $O_2$. Fig. 4a gives the corresponding polarization curves, showing that $CoSe_2$/CNTs requires a low overpotential of 300 mV to achieve 10 mA/cm$^2$ with respect to bare $CoSe_2$ (350 mV). The value is also superior to many reported $CoSe_2$-based eletrocatalysts (Table S2 in supporting information). The intrinsic kinetic of OER was verified by calculating the Tafel slopes of catalysts on polarization curves (Fig. 4b), in which $CoSe_2$/CNTs shows the smaller Tafel slope of 62 mV/dec than $CoSe_2$ (92 mV/dec). Fig. S5b

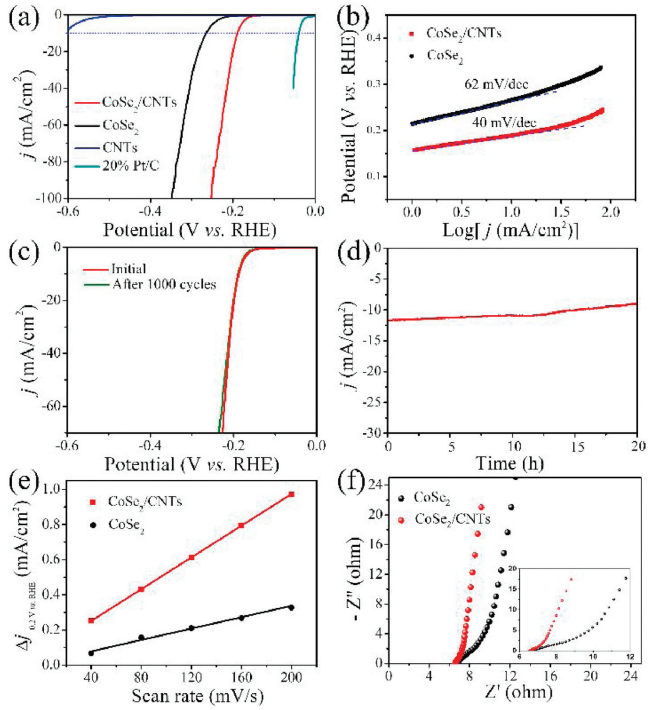


**Fig. 3.** (a) LSV polarization curves of HER for $CoSe_2$/CNTs, $CoSe_2$, CNTs, and Pt/C, in 1 mol/L KOH at a scan rate of 10 mV/s. (b) The corresponding Tafel plots of $CoSe_2$ and $CoSe_2$/CNTs. (c) LSV polarization curves recorded at $CoSe_2$/CNTs electrode with a sweep rate of 10 mV/s before and after 1000 consecutive cycles between −0.4 V and +0.3 V *vs.* RHE at 100 mV/s (with iR compensated). (d) Time-dependent current density curves of the $CoSe_2$/CNTs under a static potential of -0.16 V *vs.* RHE for 20 h. (e) The plots of corresponding current density against scan rate over $CoSe_2$ and $CoSe_2$/CNTs. (f) EIS Nyquist plots of $CoSe_2$ and $CoSe_2$/CNTs.

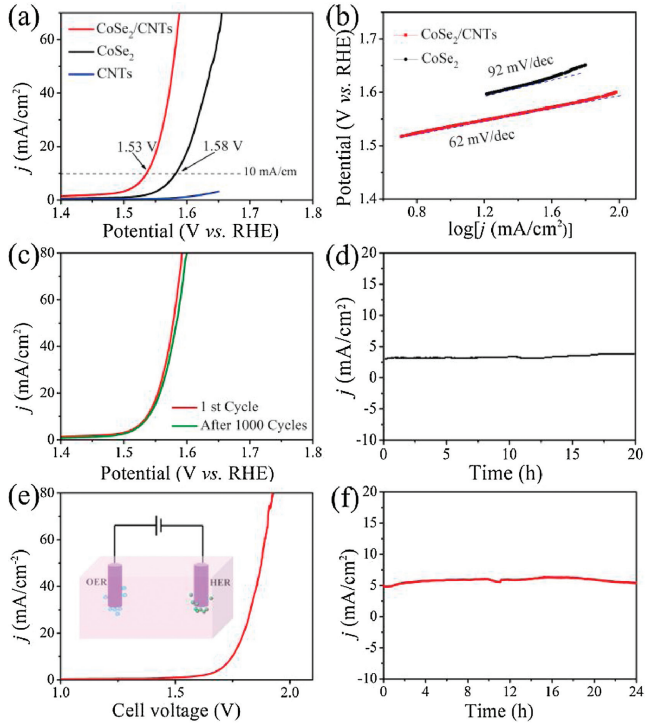


**Fig. 4.** (a) LSV polarization curves of OER for $CoSe_2$/CNTs, $CoSe_2$ and CNTs in 1 mol/L KOH at scan rate of 10 mV/s; (b) the corresponding Tafel plots of $CoSe_2$ and $CoSe_2$/CNTs. (c) LSV polarization curves recorded at $CoSe_2$/CNTs electrode with a sweep rate of 10 mV/s before and after 1000 consecutive cycles between +0.9 V and +1.8 V *vs.* RHE at 100 mV/s (with iR compensated). (d) Time-dependent current density curves of the $CoSe_2$/CNTs under a static potential of +1.5 V *vs.* RHE for 20 h. (e) Polarization curves recorded at a scan rate of 10 mV/s in a two-electrode $CoSe_2$/CNTs-based water electrolyzer. (f) Time-dependent current density curves of the $CoSe_2$/CNTs-based water electrolyzer under a static potential of 1.71 V for 24 h.

(Supporting information) shows the OER overpotentials of the $CoSe_2$ with different contents of CNTs. It can be seen that lower CNTs content is not enough for the construction of conductive network, while excessive use of CNTs is not conducive to the exposure of active sites. Therefore, a moderate ratio of CNTs to $CoSe_2$ is vital to realize a desirable electrochemical performance. To test the stability of $CoSe_2$/CNTs for OER, the LSV polarization curves of $CoSe_2$/CNTs electrode before and after 1000 consecutive cycles were recorded (Fig. 4c). After 1000 CV scans, the LSV curve of $CoSe_2$/CNTs increased by only 10 mV even at current density of 80 mA/cm$^2$ compared with the original one. Meanwhile, the electrocatalytic activity can be maintained at least 20 h at a static potential of 1.5 V *vs.* RHE, indicating its good stability for OER (Fig. 4d). The chemical changes of $CoSe_2$/CNTs nanocomposites during the OER reaction were investigated by corresponding XPS measurements. As shown in Fig. S8 (Supporting information), the intensity of Co-Se bonds was decreased after OER, while the signal of Co-O bonds at high binding energies increased greatly, implying the *in-situ* formation of cobalt oxides or CoOOH including high valence Co(III) or Co(IV) ions during the OER process [29,30]. The XPS analysis of the $CoSe_2$/CNTs nanocomposites after OER cycling shows that intermediate of CoOOH was *in-situ* formed on the $CoSe_2$ surface during the reaction.

For practical applications, we further examined its overall water splitting performance. Fig. S9 (Supporting information) shows the LSV polarization curves of the HER and OER in 1 mol/L KOH over $CoSe_2$/CNTs electrode. The onset potentials towards HER and OER are −114 mV and +1302 mV *vs.* RHE, respectively. In a two-electrode $CoSe_2$/CNTs-based water electrolyzer, the overall reaction reached at a cell voltage of 1.75 V at 10 mA/cm$^2$ (Fig. 4e), which is better than other reported similar materials (Table S3 in Supporting information). The long-term test at 1.71 V showed good stability of $CoSe_2$/CNTs electrode for water splitting (Fig. 4f).

In summary, we have developed an *in-situ* selenization route for the conversion of CNTs decorated Co-MOF nanosheets to ultrathin $CoSe_2$/CNTs nanocomposites. Since the synergistic effect between ultrathin $CoSe_2$ nanosheets with exposed active sites and CNTs with improved conductivity, the $CoSe_2$/CNTs nanocomposites exhibited good electrocatalytic activity and durability for HER and OER. Furthermore, as a bifunctional electrocatalyst, it also exhibited good overall water splitting performance. The present work provides a strategy for the fabrication of electrocatalysts for water splitting and alternative applications.

## Declaration of competing interest

The authors declare that they have no known competing financial interests or personal relationships that could have appeared to influence the work reported in this paper.

## Acknowledgments

The authors gratefully acknowledge the financial support by the National Natural Science Foundation of China (No. 21771137), the Key Project of Natural Science Foundation of Tianjin (No. 18JCZDJC97200), the Training Project of Innovation Team of Colleges and Universities in Tianjin (No. TD13-5020), and the start-up fund of Qilu University of Technology, Shandong Academy of Sciences.

## Appendix A. Supplementary data

Supplementary material related to this article can be found, in the online version, at doi:https://doi.org/10.1016/j.cclet.2020.02.029.

## References

[1] C. Hu, L. Zhang, J. Gong, Energy Environ. Sci. 12 (2019) 2620–2645.
[2] X.X. Chen, X.J. Zhen, H.Y. Gong, et al., Chin. Chem. Lett. 30 (2019) 681–685.
[3] H. Zhou, Y. Wang, R. He, et al., Nano Energy 20 (2016) 29–36.
[4] S. Bai, C. Wang, M. Deng, et al., Angew. Chem. Int. Ed. 53 (2014) 12120–12124.
[5] N. Cheng, S. Stambula, D. Wang, et al., Nat. Commun. 7 (2016) 13638.
[6] Y. Lee, J. Suntivich, K.J. May, E.E. Perry, Y. Shao-Horn, J. Phys, Chem. Lett. 3 (2012) 399–404.
[7] D. Kiriya, P. Lobaccaro, H.Y.Y. Nyein, et al., Nano Lett. 16 (2016) 4047–4053.
[8] G.J. Wei, Z.J. Wang, X.X. Zhao, et al., Mater. Res. Express 2 (2014) 015501.
[9] J. Ran, J. Zhang, J. Yu, M. Jaroniec, S.Z. Qiao, Chem. Soc. Rev. 43 (2014) 7787–7812.
[10] D.D. Wang, Y.Q. Zou, L. Tao, et al., Chin. Chem. Lett. 30 (2019) 826–838.
[11] D. Merki, X. Hu, Energy Environ. Sci. 4 (2011) 3878–3888.
[12] D.H. He, X.L. Wu, W. Liu, et al., Chin. Chem. Lett. 30 (2019) 229–233.
[13] J. Suntivich, K.J. May, H.A. Gasteiger, J.B. Goodenough, Y. Shao-Horn, Science 6061 (2011) 1383–1385.
[14] Y. Liu, H. Cheng, M. Lyu, et al., J. Am. Chem. Soc. 136 (2014) 15670–15675.
[15] J.K. Kim, G.D. Park, J.H. Kim, S.K. Park, Y.C. Kang, Small 13 (2017) 1700068.
[16] G.J. Wei, Z. Zhou, X.X. Zhao, W.Q. Zhang, C.H. An, ACS Appl. Mater. Interfaces 10 (2018) 23721–23730.
[17] S. Peng, X. Han, L. Li, et al., Small 12 (2016) 1359–1368.
[18] R.J. Wu, M. Liu, Y.W. Peng, et al., Chin. Chem. Lett. 30 (2019) 989–994.
[19] H. Yuan, J. Li, C. Yuan, Z. He, ChemElectroChem 1 (2014) 1828–1833.
[20] S.K. Park, J.K. Kim, Y.C. Kang, Chem. Eng. J. 328 (2017) 546–555.
[21] G.D. Park, Y.C. Kang, Chem. Eur. J. 22 (2016) 4140–4146.
[22] C. Xia, Q. Jiang, C. Zhao, M.N. Hedhili, H.N. Alshareef, Adv. Mater. 28 (2016) 77–85.
[23] D. Kong, H. Wang, Z. Lu, Y. Cui, J. Am. Chem. Soc. 136 (2014) 4897–4900.
[24] Y.Y. Yao, H.J. Chao, T.H. Chou, et al., Sol. Energy 137 (2016) 401–408.
[25] S.H. Choi, Y.C. Kang, Nanoscale 8 (2016) 4209–4216.
[26] N. Kaeffer, M. Chavarot-Kerlidou, V. Artero, Acc. Chem. Res. 48 (2015) 1286–1295.
[27] H. Zhang, Y. Li, G. Zhang, et al., J. Mater. Chem. A 3 (2015) 6306–6310.
[28] X. Zhao, W. Wang, Z. Hou, et al., Inorg. Chem. Front. 6 (2019) 473–476.
[29] Y. Zhang, Y. Qiu, X. Ji, et al., ChemSusChem 12 (2019) 3792–3800.
[30] Y. Chen, S. Xu, S. Zhu, et al., Nano Res. 12 (2019) 2259–2267.